Table IV. Structural Data for Terminal Isocyanide Ligands in Various Complexes

complex	Nb-C, Å	C-N, Å	C-N-C, deg	ref
$NbCl(CO)(t\text{-BuNC})(dmpe)_2$	2.054 (7)	1.186 (8)	1.441 (7)	*a*
$[(\eta^5\text{-Cp})NbCl(t\text{-BuNC})_4]^+$	2.203 (9)-2.210 (10)	1.133 (12)-1.139 (13)	171.0 (10)-174.3 (10)	3
$Nb_2Cl_6(t\text{-BuNC})_6$	2.226 (13)-2.299 (14)	1.12 (2)-1.151 (15)	169 (1)-178 (2)	4
$Nb_3Cl_8(t\text{-BuNC})_5$	2.202 (12)-2.266 (13)	1.116 (13)-1.173 (14)	173 (1)-178 (1)	5

[a] This work.

bending of the RNC ligand. Relevant interatomic distances and angles are collected in Table III. No short contacts are observed.

The structure is best described as a monocapped-trigonal-prismatic coordination polyhedron with the chlorine in the capping position, the phosphorus atoms in the capped quadrilateral face, and the π-acceptor carbonyl and isocyanide ligands on the remaining edge. It shows similarities with the geometry of $Nb(OArMe_2\text{-}3,5)(CO)_2(dmpe)_2$[8] and that of $TaCl(CO)_3(PMe_3)_3$.[9]

The salient features of the structure appear in the form of a severe bending in the C-N-C linkage, a fairly short Nb-C bond length, and a long Nb-Cl bond length. Table IV lists the data for the structurally characterized niobium isocyanide complexes. The reduced Nb-C-N bond angle (144.1 (7)°) as well as the short Nb-C bond length (2.054 (7) Å) accounts for a carbene-like isocyanide moiety:[10,11]

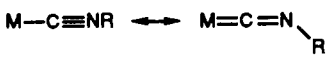

This Nb-C distance is much shorter than the values usually found for single order niobium-carbon bonds (~2.32 Å) and is in agreement with the distances observed for niobium metallocyclopropenes[12] or in tantalum alkylidenes[13] (1.93-2.07 Å). Back-bonding into one π^* bonding orbital of *t*-BuNC is favored by the low oxidation state of the metal as well as by the presence of the dmpe ligands in the coordination sphere. This bent tBuNC ligand thus accounts for the low ν(NC) frequency in the IR, as opposed to the typical values found for niobium complexes having almost linear isocyanide ligands (2185-2048 cm^{-1}, for instance, for $[(\eta^5\text{-Cp})Nb(t\text{-BuNC})_4Cl]^+$[3]). Bent terminal isocyanide ligands have also been proposed for the $(\eta^5\text{-Cp})_2MR'(RNC)$ complexes (M = Nb, Ta),[14] although no structural characterization was achieved.

The Nb-Cl bond distance of 2.627 (2) Å is unusually long and is even significantly longer than the greatest value reported for a terminal Nb-Cl bond (2.505 (4) Å).[3] Comparison of the Nb-Cl bond lengths in various derivatives reveals a progressive lengthening as the metal oxidation state decreases from 5 to 4 and to 3.[3] $NbCl(CO)(t\text{-BuNC})(dmpe)_2$ is to our knowledge the first structurally characterized mononuclear niobium(I) chlorine derivative reported so far.

The geometry observed for the diphosphine is similar to that frequently found for this ligand:[13,15,16] Pb-Nb-P bite angles of 74.08 (7) and 74.22 (8)° with Nb-P bond lengths ranging from 2.552 (2) to 2.607 (2) Å.

Acknowledgment. We are grateful to Dr. R. Astier for X-ray data collection and to Professor D. Grandjean for the use of the PDP/60 computer.

Supplementary Material Available: Tables of crystal data, intermolecular distances and angles, and anisotropic temperature parameters (3 pages); a listing of observed and calculated structure factor amplitudes (14 pages). Ordering information is given on any current masthead page.

(8) Coffindaffer, T. W.; Rothwell, I. P.; Folting, K.; Huffman, J. C.; Sterb, W. E. *J. Chem. Soc., Chem. Commun.* **1985**, 1519.
(9) Luetkens, M. L.; Santure, D. J.; Huffman, J. C.; Sattelberger, A. P. *J. Chem. Soc., Chem. Commun.* **1985**, 552.
(10) Yamamoto, Y. *Coord. Chem. Rev.* **1980**, *32*, 193.
(11) Singleton, E.; Oosthuizen, H. E. *Adv. Organomet. Chem.* **1983**, *22*, 209.
(12) Hey, E.; Weller, F.; Dehnicke, K. *Z. Anorg. Allg. Chem.* **1984**, *514*, 25.
(13) Holloway, C. E.; Melnik, M. *J. Organomet. Chem.* (a) **1986**, *303*, 1. (b) Idem *J. Organomet. Chem.* **1986**, *303*, 39.
(14) Klazinga, A. H.; Teuben, J. H. *J. Organomet. Chem.* **1980**, *192*, 75.
(15) Meakin, P.; Guggenberger, L. J.; Tebbe, F. N.; Jesson, J. P. *Inorg. Chem.* **1974**, *13*, 1025.
(16) Albright, J. O.; Datta, S.; Dezube, B.; Kouba, J. K.; Marynick, D. S.; Wreford, S. S.; Foxman, B. M. *J. Am. Chem. Soc.* **1979**, *101*, 611. Bianconi, P. A.; Williams, I. D.; Engeler, M. P.; Lippard, S. J. *J. Am. Chem. Soc.* **1986**, *108*, 311.

Contribution from the Institut für Organische Chemie, Universität Erlangen-Nürnberg, Henkestrasse 42, D-8520 Erlangen, Germany, Institute of Organic Chemistry and Biochemistry, Czechoslovak Academy of Sciences, 16618 Prague 6, CSFR, and Institute of Inorganic Chemistry, Czechoslovak Academy of Sciences, 25068 Řež near Prague, CSFR

On the Origin of the Antipodal Effect in *closo*-Heteroboranes

M. Bühl,[†] P. v. R. Schleyer,*[,†] Z. Havlas,[‡] D. Hnyk,[§] and S. Heřmánek[§]

Received November 27, 1990

Introduction

One of the main factors governing the ^{11}B chemical shifts in heteroboranes is the "antipodal" effect or A-effect.[1,2] The replacement of a boron nucleus in a polyhedral borane by a heteroatom (or group) X results in a downfield $\delta(^{11}B)$ chemical shift for the boron across the cage from X. Even though farthest away, the antipodal boron often undergoes the largest chemical shift change of all nuclei that are influenced by X.

The origin of the A-effect has been the topic of several empirical[1,2] and theoretical[3,4] investigations. Heřmánek, Hnyk, and Havlas (HHH) noticed a linear correlation of $\delta(^{11}B)$ of the antipodal atom in 10- and 12-vertex cages with *p* densities (charges) obtained from CNDO/2 calculations.[3] Fehlner, Czech, and Fenske (FCF) compared the paramagnetic chemical shift components in $B_{10}H_{10}^{2-}$ and B_9H_9NH employing the Fenske-Hall MO method.[4] They ascribed the enhanced paramagnetic (deshielding) contributions in the aza compound to a smaller energetic difference ΔE between suitable occupied and unoccupied MO's and to a larger "antipodal B-" character of these MO's with respect to the boron homologue.

We have been using the IGLO (individual gauge for localized orbitals) method[5] to calculate ^{11}B chemical shifts for boron compounds.[6] Remarkable precision can be achieved provided accurate geometries are employed.

Our objective was to test if IGLO calculations at a modest level of theory could reproduce the large chemical shift differences associated with the antipodal effect. In addition, we expected further information concerning the origin of this effect. The largest

[†] Universität Erlangen-Nürnberg.
[‡] Institute of Organic Chemistry and Biochemistry, Czechoslovak Academy of Sciences.
[§] Institue of Inorganic Chemistry, Czechoslovak Academy of Sciences.

0020-1669/91/1330-3107$02.50/0

Table I. Geometries and IGLO ^{11}B NMR Chemical Shifts for B_9H_9X Compounds [Distances in Å; 3-21G(*) Optimized; $\delta(^{11}B)$ Values in ppm Relative to $BF_3{\cdot}OEt_2$; DZ//3-21G(*) Level] with Experimental Chemical Shifts in Italics[a]

	X									
distance	BH^{2-} [b]	AlH^{2-}	CH^-	SiH^-	N^-	P^-	NH	PH	O	S[c]
XB(2)	1.720	2.105	1.623	1.984	1.593	1.970	1.616	1.938	1.613	1.962
B(2)B(3)	1.875	1.933	1.882	1.974	1.864	1.925	1.923	2.027	1.937	1.987
B(2)B(6)	1.846	1.841	1.834	1.831	1.835	1.825	1.817	1.822	1.813	1.808
B(6)B(7)	1.875	1.880	1.880	1.883	1.879	1.878	1.889	1.891	1.891	1.887
B(6)(B10)	1.720	1.718	1.721	1.715	1.723	1.718	1.729	1.722	1.732	1.728
	X									
$\delta(^{11}B)$	BH^{2-}	AlH^{2-}	CH^-	SiH^-	N^-	P^-	NH	PH	O	S
B(2-5)	-26.9	-37.2	-14.7	-27.9	-5.3	-9.6	2.5	-8.0	15.8	9.6
	-28.0		*-20.0*		*-8.3*		*-6.1*			*-4.8*
B(6-9)	-26.9	-31.4	-21.2	-24.3	-14.7	-18.6	-16.1	-22.6	-11.7	-12.7
	-28.0		*-24.1*		*-18.3*		*-21.5*			*-17.6*
B(10)	-6.8	-26.4	32.2	12.4	45.8	40.7	65.6	49.8	78.6	80.4
	-2.0		*28.4*		*50*		*61*			*74.5*

[a] From refs 7-10. [b] The averaged experimental distances in $Cu_2B_{10}H_{10}$ are B(1)B(2) = 1.73, B(2)B(3) = 1.86, and B(2)B(6) = 1.81 Å: Dobrott, R. D.; Lipscomb, W. N. *J. Chem. Phys.* **1962**, *37*, 1779. [c] Cf. the averaged experimental distances in 2,2'-(1-$SB_9H_8)_2$: SB(2) = 1.923, B(2)B(3) = 1.928, B(2)B(6) = 1.780, B(6)B(7) = 1.842, and B(6)B(10) = 1.693 Å.[16]

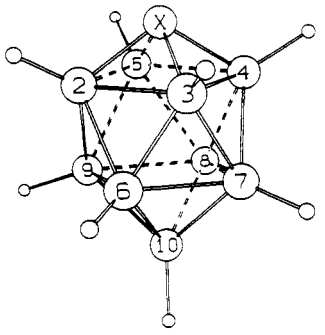

Figure 1. Molecular skeleton and numbering scheme for *closo*-B_9H_9X compounds.

effect is observed for the antipodal boron B(10) in the 10-vertex series B_9H_9X ($\delta(^{11}B)$ = -2.0,[7] 28.4,[8] 50,[9] 61,[9] and 74.5[10] ppm for X = BH^{2-}, CH^-, N^-, NH, and S, respectively). The maximum difference is nearly 80 ppm! Hence, we chose this system for a systematic investigation. We now report ab initio optimized geometries and calculated chemical shifts for this series, with X ranging from BH^{2-} to O and from AlH^{2-} to S.

Methods

The geometries were fully optimized in C_{4v} symmetry ($B_{10}H_{10}^{2-}$: D_{4d}) by employing CADPAC[11] with the standard 3-21G(*) basis set[12] (same as 3-21G, but augmented with polarization functions for the second-row elements). The chemical shifts were calculated by using the IGLO program[5] employing a double-ζ (DZ) basis set of Huzinaga.[13] Gaussian lobes contracted as follows:[5b] B, C, N, and O, 7s3p (4111/21); Al, Si, P, and S, 10s6p (511111/3111); H, 3s (21). The principal components of the chemical shielding σ are computed with respect to the bare nucleus;[14] relative chemical shifts δ are referred to $BF_3{\cdot}OEt_2$.[15]

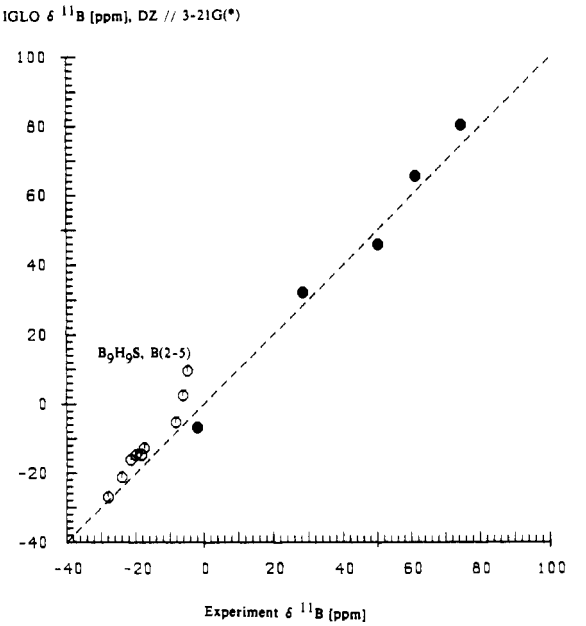

Figure 2. Plot of IGLO [DZ//3-21G(*)] vs experimental ^{11}B chemical shifts for B_9H_9X compounds. The ideal slope = 1 is given. ● denotes antipodal borons B(10).

Results and Discussion

Computed geometries and ^{11}B chemical shifts are summarized in Table I (for the numbering scheme, see Figure 1). The most pronounced geometric distortion induced by the heterovertex X is the elongation of the adjacent tetragonal belt, e.g. B(2)B(3) = 1.875 and 1.987 Å for X = BH^{2-} and S,[16] repectively. A similar

(1) (a) Plešek, J.; Heřmánek, S. *J. Chem. Soc., Chem. Commun.* **1975**, 127. (b) Heřmánek, S.; Gregor, V.; Štibr, B.; Plešek, J.; Janousek, Z.; Antonovich, V. A. *Coll. Czech. Chem. Commun.* **1976**, *41*, 1492. (c) Heřmánek, S., Jelínek, T., Plešek, J., Štibr, B., Fusek, J., Mareš, F. In *Boron Chemistry, Proceedings of the 6th IMEBORON*; Heřmánek, S., Ed.; World Scientific: Singapore, 1987; pp 26-73.
(2) (a) Todd, L. J.; Siedle, A. R.; Bodner, G. M.; Kahl, S. B.; Hicke, J. P. *J. Magn. Reson.* **1976**, *23*, 301. (b) Leyden, R. N.; Sullivan, B. P.; Baker, R. T.; Hawthorne, M. F. *J. Am. Chem. Soc.* **1978**, *100*, 3758. (c) Teixidor, F.; Vinas, C.; Rudolph, R. W. *Inorg. Chem.* **1986**, *25*, 3339.
(3) Heřmánek, S.; Hnyk, D.; Havlas, Z. *J. Chem. Soc., Chem. Commun.* **1989**, 1895.
(4) Fehlner, T. P.; Czech, P. T.; Fenske, R. F. *Inorg. Chem.* **1990**, *29*, 3103.
(5) (a) Kutzelnigg, W. *Isr. J. Chem.* **1980**, *19*, 193. (b) Schindler, M.; Kutzelnigg, W. *J. Chem. Phys.* **1982**, *76*, 1919. Review: (c) Kutzelnigg, W.; Fleischer, U.; Schindler, M. In *NMR, Basic Principles and Progress*; Springer Verlag: Berlin, 1990; p 165.
(6) (a) Schleyer, P. v. R.; Bühl, M.; Fleischer, U.; Koch, W. *Inorg. Chem.* **1990**, *29*, 153. (b) Schleyer, P. v. R.; Bühl, M. *Angew. Chem., Int. Ed. Engl.* **1990**, *29*, 304. (c) Bühl, M.; Schleyer, P. v. R. *Angew. Chem., Int. Ed. Engl.* **1990**, *29*, 886. (d) Bühl, M.; Schleyer, P. v. R. In *Electron Deficient Boron and Carbon Clusters*; Olah, G. A., Wade, K., Williams, R. E., Eds.; Wiley: New York, 1990; Chapter 4, p 113.
(7) Hawthorne, M. F.; Pilling, R. L.; Stokely, P. F. *J. Am. Chem. Soc.* **1965**, *87*, 1893.
(8) Knoth, W. J. *J. Am. Chem. Soc.* **1967**, *89*, 1274.
(9) Arafat, A.; Baer, J.; Huffmann, J. C.; Todd, L. J. *Inorg. Chem.* **1986**, *25*, 3757.
(10) Rudolph, R. W.; Pretzer, W. R. *J. Am. Chem. Soc.* **1973**, *95*, 931.
(11) Amos, R. D.; Rice, J. E. CADPAC: The Cambridge Analytical Derivatives Package, Issue 4.0. Cambridge, 1987.
(12) Hehre, W.; Radom, L.; Schleyer, P. v. R.; Pople, J. A. *Ab Initio Molecular Orbital Theory*, Wiley: New York, 1986.
(13) Huzinaga, S. *Approximate Atomic Wave Functions*; University of Alberta: Edmonton, Canada, 1971.
(14) Note the different sign convention: larger σ values denote larger shielding!
(15) B_2H_6 was used as the primary reference; cf. discussion in ref 6d.
(16) Pretzer, W. R.; Hilty, T. K.; Rudolph, R. W. *Inorg. Chem.* **1975**, *14*, 2459.

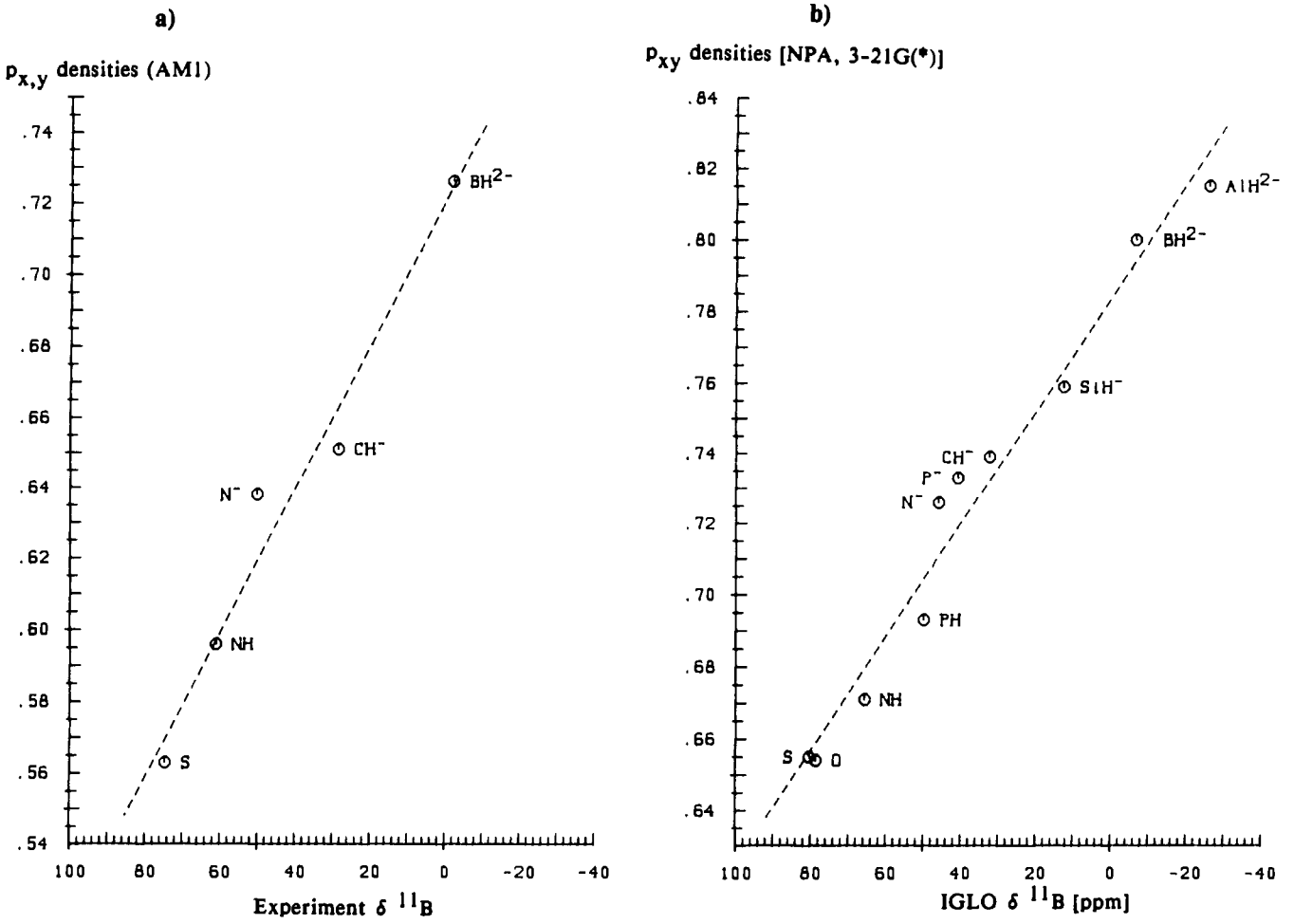

Figure 3. Correlations of the "antipodal" ^{11}B chemical shifts with the occupancies of the p_x and p_y orbitals of B(10) in the B_9H_9X series (perpendicular to the molecular axis taken as z): (a) AM1 densities vs experimental chemical shifts (cf. ref 3); (b) NPA densities [3-21G(*) level] vs IGLO chemical shifts [DZ//3-21G(*)].

effect has been observed in 12-vertex cages.[17] Note that the "local geometry" around the critical boron B(10) (i.e. bond distances B(6)B(7) and B(6)B(10); see Table I) is practically unaffected by the heteroatom.

The IGLO $\delta(^{11}B)$ values are in rather good accord with the experimental chemical shifts when available (Table I). Least-squares analysis of calculated vs experimental $\delta(^{11}B)$ values (plotted in Figure 2) affords a slope of 0.98 with a standard deviation of 4.7 ppm and a correlation coefficient of 0.990. This is comparable to the degree of agreement achieved for binary boron hydrides at the same level of theory.[6d] The largest deviation from experiment, ca. 14 ppm, is found for B(2-5) in B_9H_9S. This is probably due to the poor description of the adjacent sulfur by the DZ basis.[18] The trend in $\delta(^{11}B)$ of the antipodal B(10) (● in Figure 2), however, is nicely reproduced by the calculations. The B(10) $\delta(^{11}B)$ values predicted for the second-row heteroatoms X = AlH^{2-}, SiH^-, P^-, and PH are somewhat shifted to higher field when compared to their first-row homologues (cf. the $\delta(^{11}B)$ values for B(12) of −14.9[19] and −25.1[20] ppm in $B_{12}H_{12}^{2-}$ and $B_{11}H_{11}AlMe^{2-}$, respectively).

Table II. Tensor Components $\sigma_\perp$ and $\sigma_\parallel$ for the Shielding of B(10) in B_9H_9X Compounds [in ppm, IGLO DZ//3-21G(*)]

	X				
	BH^{2-}	CH^-	N^-	NH	O
$\sigma_\perp$	148	130	120	113	108
$\sigma_\parallel$	120	39	17	−29	−57
	X				
	AlH^{2-}	SiH^-	P^-	PH	S
$\sigma_\perp$	162	141	113	117	89
$\sigma_\parallel$	151	76	47	11	−25

Attempts to correlate ^{11}B chemical shifts with calculated atomic charges have met with variable success.[3,6d,21] Figure 3 shows correlations of the ^{11}B chemical shifts with the occupancies of the B(10) p_x and p_y orbitals (perpendicular to the molecular axis taken as z). In the left-hand part (Figure 3a), AM1[22] densities are plotted vs experimental chemical shifts (cf. the analogous correlation of HHH[3]), whereas in the right hand part (Figure 3b), p_{xy} densities obtained by natural population analysis (NPA)[23] are correlated with the IGLO $\delta(^{11}B)$ values. Linear relations are apparent, essentially confirming the results of HHH,[3] which were based on CNDO/2 calculations. The correlation of the B(10) chemical shifts with the total atomic (NPA) charges as shown

(17) Hnyk, D.; Vajda, E.; Bühl, M.; Schleyer, P. v. R. Submitted for publication.
(18) Schindler, M. *J. Chem. Phys.* **1988**, *88*, 7638; Unfortunately, the molecules of this study are too big for calculations with larger basis sets including polarization functions. We did not test the effect of a single d function for the second-row elements; however, for chlorine compounds such a "slightly extended" DZ basis gave no significantly better results: Fleischer, U. Private communication.
(19) (a) Hawthorne, M. F.; Pitochelli, A. R. *J. Am. Chem. Soc.* **1960**, *82*, 3228. (b) Srebny, H. G.; Preetz, W.; Marsman, H. C. *Z. Naturforsch.* **1984**, *39B*, 189.
(20) Getman, T. D.; Shore, S. G. *Inorg. Chem.* **1988**, *27*, 3439.
(21) (a) Kroner, J.; Wrackmeyer, B. *J. Chem. Soc. Faraday Trans. 2* **1976**, *72*, 2283. (b) Kroner, J.; Nölle, D.; Nöth, H. *Z. Naturforsch.* **1973**, *28B*, 416.
(22) Dewar, M. J. S.; Zoebisch, E. G.; Healy, E. A.; Stewart, J. J. P. *J. Am. Chem. Soc.* **1985**, *107*, 3902.
(23) Reed, A. E.; Weinstock, R. B.; Weinhold, F. *J. Chem. Phys.* **1985**, *83*, 735.

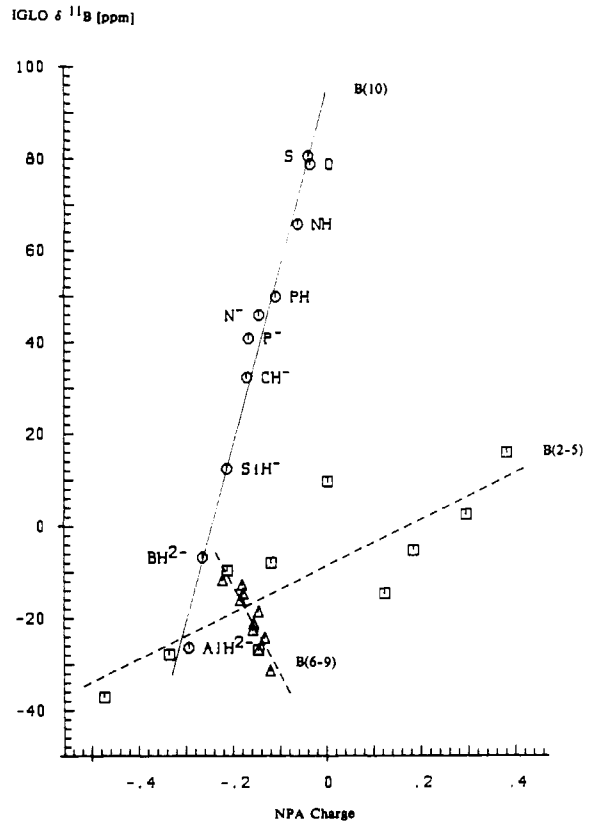

Figure 4. Correlation of IGLO ^{11}B chemical shifts [DZ//3-21G(*)] with total atomic (natural) charges [3-21G(*) level] for the various boron nuclei in B_9H_9X compounds: (□) B(2-5), (△) B(6-9); (○) B(10).

in Figure 4 obviously is excellent as well.[24] However, the analogous plots for the remaining boron atoms B(2–5) and B(6–9), which are included in Figure 4, demonstrate that there is no common basic relation between charge and chemical shift. In the case of B(6–9), the slope even is negative; i.e. a more positive charge is associated with a shift to higher field. The question is, why does $\delta(^{11}B)$ of B(10) seem to be so susceptible to charge effects; i.e. why is the corresponding slope in Figure 4 (ca. 380 ppm per electron!) so large?

As pointed out by FCF,[4] the deshielding of B(10) in B_9H_9NH with respect to $B_{10}H_{10}^{2-}$ is due to the change in σ_p, the paramagnetic part of the chemical shielding. The computed principal values of the chemical shielding tensor, $\sigma_\parallel$ and $\sigma_\perp$ (parallel and perpendicular to the molecular axis, respectively; see Table II) reveal a considerable anisotropy of the chemical shift. The largest variation is found for $\sigma_\parallel$. This differs e.g. for X = BH^{2-} and NH by ca. 150 ppm, thereby accounting for roughly 70% of the overall change in $\delta(^{11}B)$ (the difference in the two equivalent $\sigma_\perp$ values is 2 × 35 = 70 ppm). Except perhaps for X = S, the $\sigma_\perp$ values for the corresponding first- and second-row elements are indicated to be very similar.

The strongly deshielding effect parallel to the molecular axis (z axis) may be assigned to the coupling of occupied and unoccupied MO's with p_x and p_y character on B(10). Hence, the term "NMR-active orbitals" introduced by HHH[3] is justified. With the exception of $B_{10}H_{10}^{2-}$, the degenerate HOMO and LUMO pairs have the correct symmetry to give rise to paramagnetic contributions. This is in accord with the approach of FCF,[4] who conclude that the enhanced paramagnetic contributions in B_9H_9NH originate in a smaller ΔE between HOMO and LUMO and in a larger B(10) character (i.e. larger p-AO coefficient) of the HOMO. Both characteristics of the whole B_9H_9X series are summarized in Table III [3-21G(*) basis set].

(24) The corresponding B(10) Mulliken charges are shifted somewhat to more positive values; the correlation with the B(10) chemical shifts is slightly worse but comparable to that shown in Figure 4.

Table III. ΔE Values[a] and 2p AO Coefficients[b] for X and B(10) of B_9H_9X Compounds [3-21G(*) Level]

	X				
	BH^{2-}	CH^-	N^-	NH	O
ΔE	13.9[c]	13.1	13.1	12.6	12.4
HOMO $p_{xy}(X)$	0.239	0.155	0.119	0.093	0.081
$p_{xy}(B)$	0.239	0.247	0.264	0.269	0.263
	X				
	AlH^{2-}	SiH^-	P^-	PH	S
ΔE	10.0	11.9	12.4	12.2	12.1[d]
HOMO $p_{xy}(X)$	0.224	0.260	0.240	0.216	0.191
$p_{xy}(B)$	0.202	0.248	0.263	0.271	0.269

[a] Energy difference in eV between the degenerate HOMO and LUMO pairs. [b] Only the coefficients of the inner orbitals of the split-valence 3-21G basis are given. [c] For $B_{10}H_{10}^{2-}$, the coupled HOMO/LUMO pairs do not contribute to σ_p due to their symmetry; hence, the energy difference between the LUMO and the next suitable occupied MO's (pair 17,18) is given; cf. ref 4. [d] For B_9H_9S, a vertical ionization potential of 10.3 eV has been measured: Fehlner, T. P.; Wu, M.; Meneghelli, B. J.; Rudolph, R. W. *Inorg. Chem.* **1980**, *19*, 49.

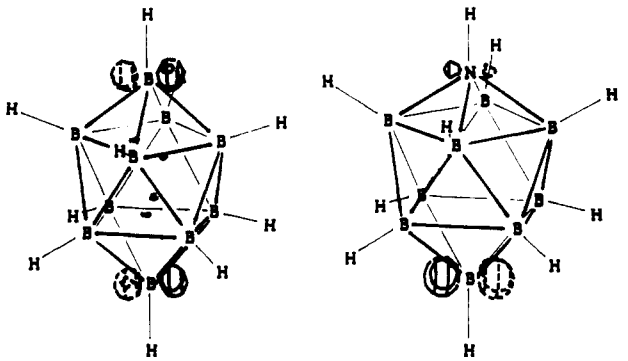

Figure 5. Jørgensen plot (STO-3G wave function) of the HOMO in $B_{10}H_{10}^{2-}$ (left) and B_9H_9N (right).

For the first-row heteroatoms, ΔE decreases somewhat from X = BH^{2-} to X = O. This is in line with the increasing paramagnetic contributions in this series. For the second-row substituents, however, the change in the computed ΔE values does not parallel the IGLO chemical shifts (Table I). ΔE increases in going from X = AlH^{2-} to X = P^- and decreases from X = P^- to X = S. In addition, the ΔE values of the second-row heteroboranes are smaller than those of the corresponding first-row homologues, although for the latter the deshielding in the z direction is larger (more negative $\sigma_\parallel$ values; cf. Table II). Hence, the variation in ΔE alone cannot account for the trends in $\delta(^{11}B)$ of B(10).

FCF noticed a larger antipodal B_{2p} character in the HOMO of B_9H_9N as compared to $B_{10}H_{10}^{2-}$.[4] This may also enhance paramagnetic contributions due to a "better overlap" between the coupled occupied and virtual MO's (implicit in typical matrix elements like $\langle\Phi_{virt}|L_{x,y,z}|\Phi_{occ}\rangle^4$). The HOMO p_x and p_y AO coefficients on X and B(10), designated $p_{xy}(X)$ and $p_{xy}(B)$, respectively, are given in Table III. Although the numerical value of $p_{xy}(B)$ hardly changes, a polarization of the HOMO is apparent: $p_{xy}(X)$ decreases significantly for the more electronegative first-row heteroatoms. This polarization is illustrated by a Jørgensen plot[25] of the HOMO for $B_{10}H_{10}^{2-}$ and B_9H_9NH (Figure 5). For the latter, the larger B_{2p} character is clearly visible. For the second-row heterovertices, this polarization is much less pronounced, which is reflected in larger $p_{xy}(X)$ coefficients. Hence, smaller paramagnetic contributions due to a less efficient overlap between the coupled HOMO and LUMO pairs are expected.

Although allowed by symmetry, this overlap is apparently close to zero for X = AlH^{2-}, since the LUMO contains practically no antipodal B character [$p_{xy}(B)$ close to zero].

(25) Jørgensen, W. L. *QCPE* **1977**, 340.

Conclusion

Enhanced paramagnetic contributions due to decreasing ΔE(HOMO–LUMO) and due to a larger antipodal B_{2p} character of the HOMO may qualitatively rationalize the computed trends in $\delta(^{11}B)$ of the antipodal boron B(10). Since the computed ΔE values do not parallel the IGLO chemical shifts of B(10), the "polarization" of the HOMO seems to be the more important factor governing the A-effect in the 10-vertex series. In contrast to FCF, we predict heterofragments of less or similar electronegativity than the borane fragment (i.e. X = SiH^- or X = PH) to cause a substantial downfield shift of the antipodal boron. In this context, it is interesting to note that the A-effect in B_9H_9Se ($\delta(^{11}B)$ of B(10) 73.3 ppm[26]) is very pronounced.

The remaining question is, why is the antipodal effect in the 10-vertex cages so large? Further studies including 12-vertex heteroboranes that might provide insights in this problem are in progress.

Acknowledgment. This work was supported by the Deutsche Forschungsgemeinschaft and the Stiftung Volkswagenwerk. We thank Professor W. Kutzelnigg and Dr. M. Schindler for the Convex version of the IGLO program (which is available for distribution) and U. Fleischer for extensive discussion and advice. M.B. acknowledges a grant of the Studienstiftung des Deutschen Volkes. The calculations were performed on a Cray Y-MP4 computer of the Leibniz Rechenzentrum Munich and on a Convex C-210s computer of the Institut für Organische Chemie.

(26) Friesen, G. D.; Kump, R. L.; Todd, L. J. *Inorg. Chem.* **1980**, *19*, 1485.

Contribution from the Department of Chemistry and Biochemistry, University of California, Los Angeles, California 90024

Luminescence from the Chair and Cube Isomers of $Ag_4I_4(PPh_3)_4$

Maher Henary and Jeffrey I. Zink*

Received July 12, 1990

The luminescence properties of tetrameric metal clusters of the type $M_4X_4L_4$ where M is a d^{10} ion such as Cu^+, Ag^+, or Au^+, X = Cl^-, Br^-, or I^-, and L is a substituted pyridine or substituted phosphine are attracting increasing attention. Reports of the luminescence of clusters containing four Ag^+ ions,[1] four Au^+ ions,[2] four Cu^+ atoms,[3-6] and mixed Cu^+/first-row transition-metal ions[7] have recently appeared.

The tetrameric clusters generally exist in either a distorted cubane geometry, consisting of a M_4X_4 core, or a distorted chair structure. Idealized forms of these structures are sketched in I and II. The steric and electronic factors that lead to these

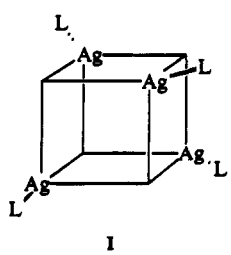

I

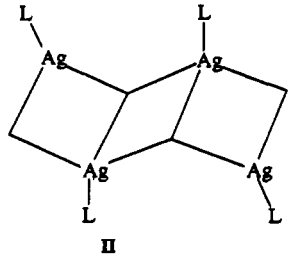

II

(1) Vogler, A.; Kunkely, H. *Chem. Phys. Lett.* **1989**, *158*, 74.
(2) Vogler, A.; Kunkely, H. *Chem. Phys. Lett.* **1988**, *150*, 135.
(3) Hardt, D. D.; Pierre, A. *Inorg. Chim. Acta* **1977**, *25*, L59.
(4) Vogler, A.; Kunkely, H. *J. Am. Chem. Soc.* **1986**, *108*, 7211.
(5) Kyle, K. R.; DiBenedetto, J.; Ford, P. C. *J. Chem. Soc., Chem. Commun.* **1989**, 714.
(6) Kyle, K. R.; Ryu, C. K.; DiBenedetto, J. A.; Ford, P. C. *J. Am. Chem. Soc.* **1991**, *113*, 2954.
(7) Henary, M.; Zink, J. I. *J. Am. Chem. Soc.* **1989**, *111*, 7407.

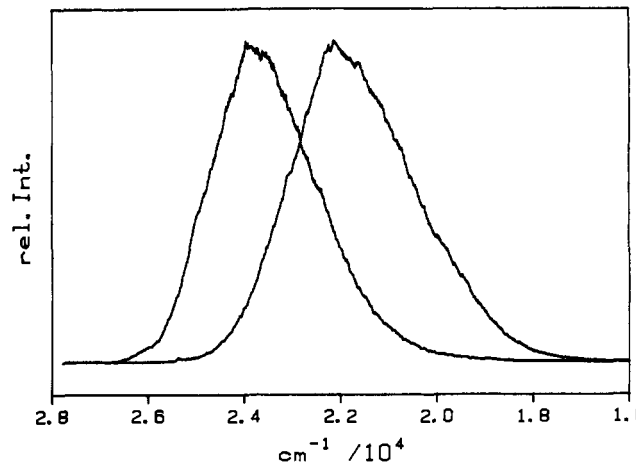

Figure 1. Luminescence spectra of solid samples of the chair (left) and the cube (right) forms of $Ag_4I_4(PPh_3)_4$ at 12 K.

geometries have been evaluated.[8] The compound $Ag_4I_4(PPh_3)_4$ is unusual because it undergoes a cube → chair isomerization and because the two geometric forms can be isolated by crystallization from different solvents.[8] It thus offers the unique opportunity to study the luminescence properties of the two isomers of the same tetrameric molecule. We report in this paper the luminescence spectra, temperature dependence, and lifetimes of the emission of the cube and chair forms of $Ag_4I_4(PPh_3)_4$.

Experimental Section

The tetrameric $Ag_4I_4(PPh_3)_4$ compound was prepared according to the literature procedure.[8] The cube isomer was prepared by crystallization from $CHCl_3/Et_2O$, and the chair isomer, by crystallization from CH_2Cl_2/Et_2O.

Emission spectra were obtained from microcrystalline samples of the compounds at temperatures between 12 and 120 K by exciting them with the 351- and 363-nm lines from an argon ion laser. The samples were mounted on an OFHC copper block in an Air Products displex closed-cycle helium refrigerator. The spectra were obtained by using a Spex 0.75-m monochromator, RCA C31034 photomultiplier, photon counting, and computer data collection.[9]

Lifetime measurements were carried out by monitoring the emission through the 0.75-m monochromator at two wavelengths, the first corresponding to the maximum of the emission band and the second to the long-wavelength side of the peak. The decay curves were recorded by using a Tektronix RTD 710 transient digitizer interfaced to a computer. The instrument response time was about 15 ns. The data were later transferred to a VAX780 computer for further processing.

Results

The 12 K luminescence spectra of the cube and chair isomers of $(Ph_3P)_4Ag_4I_4$ are shown in Figure 1. The emission maximum of the chair form at 23 900 cm^{-1} is at significantly higher energy than that of the cube form at 22 000 cm^{-1}. The fwhm for the chair is 2600 cm^{-1}, and that for the cube is 2900 cm^{-1}.

The temperature dependences of the emission spectra follow the same pattern for both isomers. As the temperature is raised, the emission intensities decrease and shift slightly to the red. When the temperature is raised to 120 K, for example, the emission intensities decrease by about a factor of 3 and the band maximum shifts by about 500 cm^{-1}.

Emission lifetimes were measured for both isomers at 15 K. The luminescence decay was monitored at the emission band maximum and at 18 000 cm^{-1} in the case of the cube and at the band maximum and 21 000 cm^{-1} in the case of the chair. The lifetime of the cube isomer is 40 ± 20 μs and that of the chair isomer is 300 ± 100 μs. A short-lived component of about 50 μs was observed in the latter case and is probably the result of a trace amount of the cube isomer in the crystals of the chair isomer. A very long-lived component (~ms) was observed in the decay curves of some samples. Free triphenylphosphine emits in the 23 000-cm^{-1}

(8) Teo, B.-K.; Calabrese, J. C. *Inorg. Chem.* **1976**, *15*, 2474.
(9) Tutt, L.; Zink, J. I. *J. Am. Chem. Soc.* **1986**, *108*, 5830.

0020-1669/91/1330-3111$02.50/0